ACS APPLIED MATERIALS & INTERFACES

Research Article

www.acsami.org

Enhanced Gas Sensing Properties of SnO_2 Hollow Spheres Decorated with CeO_2 Nanoparticles Heterostructure Composite Materials

Jiangyang Liu,[†] Mingjun Dai,[†] Tianshuang Wang,[†] Peng Sun,*[,†] Xishuang Liang,[†] Geyu Lu,*[,†] Kengo Shimanoe,[‡] and Noboru Yamazoe[‡]

[†]College of Electronic Science and Engineering, Jilin University, 2699 Qianjin Street, Changchun 130012, China

[‡]Department of Energy and Material Sciences, Faculty of Engineering Sciences, Kyushu University, Kasuga-shi, Fukuoka 816-8580, Japan

Supporting Information

ABSTRACT: CeO_2 decorated SnO_2 hollow spheres were successfully synthesized via a two-step hydrothermal strategy. The morphology and structures of as-obtained CeO_2/SnO_2 composites were analyzed by various kinds of techniques. The SnO_2 hollow spheres with uniform size around 300 nm were self-assembled with SnO_2 nanoparticles and were hollow with a diameter of about 100 nm. The CeO_2 nanoparticles on the surface of SnO_2 hollow spheres could be clearly observed. X-ray photoelectron spectroscopy results confirmed the existence of Ce^{3+} and the increased amount of both chemisorbed oxygen and oxygen vacancy after the CeO_2 decorated. Compared with pure SnO_2 hollow spheres, such composites revealed excellent enhanced sensing properties to ethanol. When the ethanol concentration was 100 ppm, the sensitivity of the CeO_2/SnO_2 composites was 37, which was 2.65-times higher than that of the primary SnO_2 hollow spheres. The sensing mechanism of the enhanced gas sensing properties was also discussed.

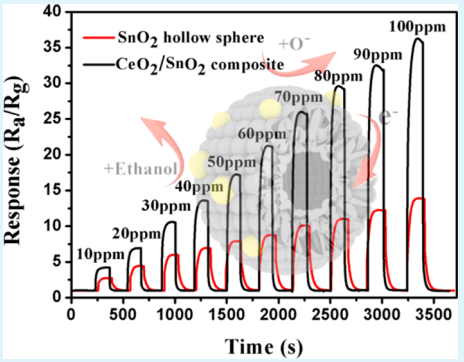

KEYWORDS: *CeO_2/SnO_2 composites, heterostructure, hollow spheres, gas sensor, sensing mechanism*

1. INSTRUCTION

As one of the predominant gas sensing materials, semiconductor oxides have captured a large amount of attention for their physical and chemical properties in the application of detecting pollutant, toxic, and explosive gases.[1−5] As we all know, surface morphology and structure of the semiconductor oxides have large effects on gas sensing properties due to the sensing mechanism, which applies the adsorption of oxygen and its reaction with test gas molecules on the surface of oxides to account for the change in resistance. Nowadays, many kinds of morphologies and structures of semiconductor oxides have been synthesized by various methods such as nanoparticles,[6] nanorods,[7] nanowires,[8] nanosheets,[9] nanospheres,[10] and nanoflowers.[11,12] Besides these, hollow nanostructures have been demonstrated to have great potential in the application of gas sensors and attracted tremendous attention owing to their high specific surface area, low density, good surface permeability, and high interfacial charge-transfer efficiency.[13−16] Up to now, the synthesis of the hollow nanostructures depends on complicated template approaches, in which hard or soft templates, for example, silica, carbon spheres, emulsion droplets, and gas bubbles, have been used. However, hollow structures prepared from template routes usually decrease the activity of sensing materials and connected with the disadvantages of tedious synthetic procedures and high cost, which may hold them back from being used in a wide range of applications. To avoid these disadvantages, hollow microstructures and nanostructures synthesized by one-step template-free method have been developed.[17]

In addition to the surface morphology and structure, classification of the materials is another main influencing factor to the gas sensing properties of semiconductor oxides. As an important n-type semiconductor with a direct band gap of 3.5 eV, SnO_2 has been regarded as the most potential sensing material because it has response to the target gases and easily for synthesizing.[18,19] However, the pure SnO_2 as sensing material has the following problems: lower response and worse selectivity. Consequently, for the purpose of increasing the sensitivity and selectivity, several approaches such as catalyst functionalization elemental doping[20−22] and heterostructure formation[23,24] have been developed. Recently, owing to the chemically distinct components in oxide semiconductor composites, it could show more excellent sensing properties than a single oxide.[25,26] Ceria, as a kind of important functional material with a direct band gap of 3.2 eV, has excellent performance in a broad range of applications involving catalysis,[27] solid oxide fuel cells,[28] oxygen sensors,[29] and chemical mechanical planarization processes.[30] For the sensors,

Received: January 6, 2016
Accepted: February 24, 2016

DOI: 10.1021/acsami.6b00169
ACS Appl. Mater. Interfaces XXXX, XXX, XXX−XXX

it has some particular characteristics, such as the outstanding oxygen storage capacity, rich oxygen vacancies, high thermal stability, and easy conversion potential between Ce^{3+} and Ce^{4+} oxidation states,[31,32] all of which make it a good candidate for gas sensing materials. Recently, many studies have demonstrated that the performance of combining SnO_2 with CeO_2 in gas sensing area. For example, Jiang et al. have synthesized Ce-doped SnO_2 thin films via the sol−gel method and dip-coating technique, which showed a high sensing property to 100 ppm butanone.[33] Porous SnO_2/CeO_2 composite NFs are synthesized using electrospinning technique, and its H_2S and ethanol gas sensing properties are investigated by Qin et al.[34] For this reason, design and synthesis of SnO_2/CeO_2 composites with novel architectures will have significant practical significance. It is expected that donated CeO_2 onto SnO_2 could improve the gas sensing properties of SnO_2 effectively.

In this paper, we report a strategy for the preparation of CeO_2/SnO_2 hollow spheres composites with uniform size by two-step hydrothermal reactions. First, the uniform size SnO_2 hollow spheres were prepared via a hydrothermal route. After that, CeO_2 nanoparticles with a diameter of ∼50 nm were decorated on the surfaces of SnO_2 hollow spheres by hydrothermal process. Moreover, CeO_2/SnO_2 hollow spheres composites successfully showed enhanced gas sensing performance to ethanol at 225 °C in comparison with pure SnO_2 hollow spheres, which demonstrate the potential application of the composites as the sensing material of a superior gas sensor. The enhanced performance may be attributed to the formation of heterojunction between the two kinds of materials as well as the redox of Ce^{3+} and Ce^{4+} states.

2. EXPERIMENTAL SECTION

2.1. Synthesis. All the reagents used in the experiment were purchased from Beijing Chemicals Co. Ltd. of China. They were all analytical grade and used directly without further purification.

2.1.1. Preparation of the Pure Hollow SnO_2 Spheres. Hollow spheres of SnO_2 were synthesized by a facile one-step hydrothermal synthesis route. The synthesis method was described as follows: 0.190 g of $SnCl_4{\cdot}6H_2O$ was dissolved in a mixture of deionized water and ethanol with the volume ratio of 1:10 followed by the addition of 0.5 mL of concentrated hydrochloric acid (mass fraction 36.5−38%) into the solution. Then the solution was ultrasonicated for 30 min for the purpose of getting a homogeneous mixture solution. After that, the final solution was transferred into a Teflon-lined stainless steel autoclave (45 mL volume) and kept at a constant temperature of 200 °C for 24 h. Then the solution temperature was decreased to room temperature naturally. The obtained white precipitate was washed alternatively with deionized water and ethanol several times by centrifugation to remove the impurity ions, and it was finally dried in vacuum at 80 °C for 12 h and calcined at 400 °C for 2 h.

2.1.2. Synthesis of the Hollow CeO_2/SnO_2 Composite Spheres. The CeO_2/SnO_2 composites were also synthesized via a simple hydrothermal method, which can be described briefly as follows: 30 mg of the obtained SnO_2 powders mentioned above was dispersed in 30 mL of deionized water under continuous magnetic stirring. Then 7.58 mg of $Ce(NO_3){\cdot}6H_2O$ and 40 mg of HMT were added into the suspension described above. After 10 min of stirring, the mixture solution was transferred into a Teflon-lined stainless steel autoclave (45 mL), sealed tightly, and maintained at 180 °C for 2 h. After that, the autoclave naturally dropped to room temperature, and the resulting products were washed with deionized water and ethanol by centrifugation. The precipitate was collected and dried at 80 °C in air for 12 h. Eventually, the CeO_2/SnO_2 composites were obtained after calcining at 400 °C for 2 h.

2.2. Characterization. Crystallinity of the as-prepared samples was characterized by X-ray powder diffraction (XRD) analysis conducted on a Rigaku D/max-2500 X-ray diffractometer with Cu−Kα (λ = 1.54178 Å) radiation 2θ ranging from 20−80° at a scanning rate of 12°/min. A JEOL JSM-7500F field-emission scanning electron microscopy (FESEM) operating at an accelerating voltage of 15 kV was directly used for determining the morphology and particle sizes of as-synthesized samples. Transmission electron microscopy (TEM), high-resolution transmission electron microscopy (HRTEM), and energy dispersive X-ray spectrometry (EDS) images patterns were recorded on a JEM-2200FS instrument (JEOL) at an accelerating voltage of 200 kV. EDS was used for measuring the chemical compositions of the products. X-ray photoelectron spectroscopy (XPS) experiments were recorded on an ESCAlab 250 Analytical XPL Spectrometer with a monochromatic Al Kα source. All the binding energies were calibrated with respect to the signal adventitious carbon C 1s peak with a binding of 284.7 eV. The fitted peaks in the XPS spectra were separated using the XPSPeak 4.1 software.

3. RESULTS AND DISCUSSION

3.1. Structural and Morphological Characteristics. The XRD pattern (Figure 1) showed the crystal structure and phase

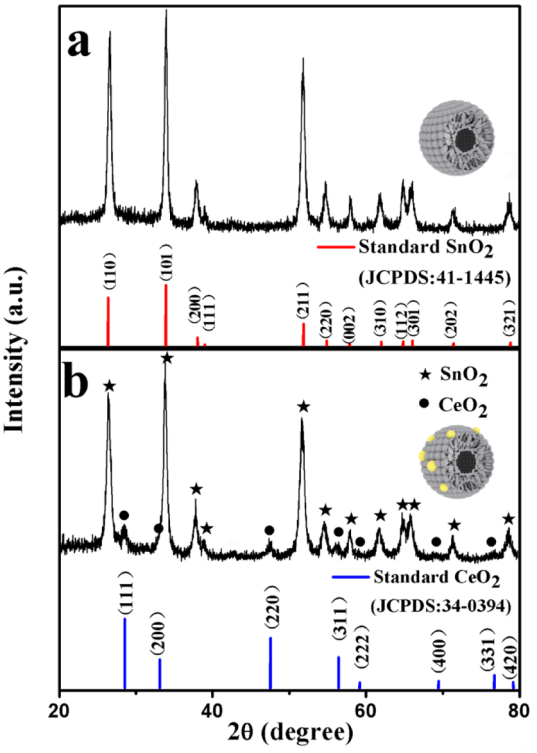

Figure 1. XRD patterns of (a) SnO_2 hollow spheres and (b) CeO_2/SnO_2 composites.

purity of as-synthesized SnO_2 hollow spheres and CeO_2/SnO_2 composites. As can be seen in the obtained XRD patterns in Figure 1, panel a, the main XRD peaks could be assigned to (110), (101), and (211), and all diffraction peaks were highly consistent with the standard XRD patterns of SnO_2 (JCPDS card no. 41−1445) with etragonal rutile structure (a = 4.738 Å, c = 3.187 Å). As for the CeO_2/SnO_2 composites, the crystal phases in Figure 1, panel b were the mixed oxides of SnO_2 and CeO_2. Apart from the peaks that belong to pure SnO_2, all the diffraction peaks left in this pattern could be assigned to the (111), (200), (220), and (311) planes indexed to fluorite cubic CeO_2 with lattice constants of a = 5.411 Å, which was consistent with the data of the standard ceria database JCPDS card no. 34−0394. Above all, no diffraction peaks belonging to

DOI: 10.1021/acsami.6b00169
ACS Appl. Mater. Interfaces XXXX, XXX, XXX−XXX

any other impurities could be detected; therefore, the high purity of the as-synthesized samples was proved.

The low-magnification FESEM image (Figure 2a) displayed a panoramic of the as-synthesized pure SnO_2, which is composed

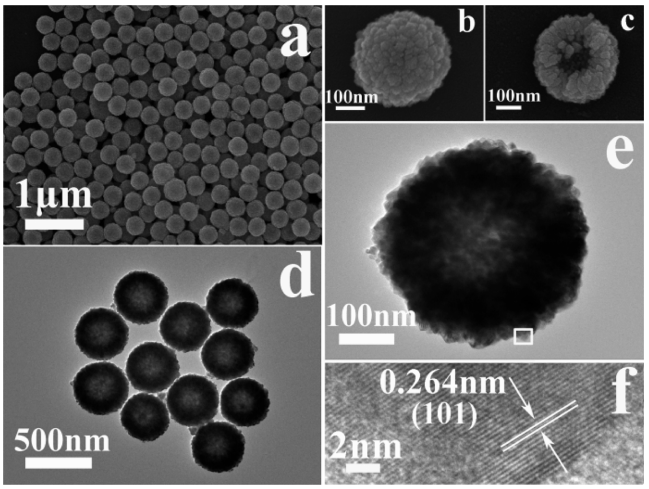

Figure 2. (a) Typical FESEM image of pure SnO_2 hollow spheres; (b, c) high-magnification FESEM images; (d, e) typical TEM images of SnO_2 hollow spheres; (f) HRTEM image obtained from the marked fringe of panel e.

of numerous spherical architectures with uniform size without other morphologies. The amplifying FESEM images in Figure 2, panel b indicated that the diameter of the obtained SnO_2 sphere was about 300 nm, and the surface was rough. The hollow structure could be clearly observed from a broken SnO_2 sphere shown in Figure 2, panel c. In addition, the shell of SnO_2 sphere was aggregated by SnO_2 nanoparticles, and the thickness was about 100 nm. The typical TEM images in Figure 2, panels d and e revealed the hollow structure of the as-synthesized SnO_2 spheres, which are in good agreement with the SEM results, while Figure 2, panel f exhibited the HRTEM image obtained from the marked fringe of the SnO_2 sphere in Figure 2, panel e. The interplanar spacing measured among adjacent lattice planes was 0.264 nm, which also belongs to the (101) crystallographic planes of rutile structure of SnO_2.

After CeO_2 was decorated on the SnO_2 hollow spheres, a typical low-magnification SEM image of the composites was shown in Figure 3, panel a, from which the CeO_2 nanoparticles could be clearly observed on the surface of SnO_2 hollow spheres, and a majority of SnO_2 hollow spheres had been composited with CeO_2 nanoparticles. Figure 3, panel b displayed detailed morphological information on a single SnO_2 hollow sphere with CeO_2 nanoparticles decorated on its surface. To further investigate the interior and the crystalline structure, the TEM and HRTEM observations were carried out. From the low-magnification TEM image of CeO_2/SnO_2 composites (Figure 3c) and the enlarged TEM observation of an individual sphere (Figure 3d), a distinct hollow interior and the CeO_2 nanoparticles could be clearly identified. The apparent lattice fringes observed from the HRTEM images (Figure 3e,f) presented that the lattice spacing of adjacent lattice planes were about 0.335 and 0.312 nm, which corresponded to the distance between the (110) plane of the tetragonal rutile structure SnO_2 (JCPDS.41−1445) and (111) plan of the fluorite cubic CeO_2 (JCPDS.34−0394), respectively.

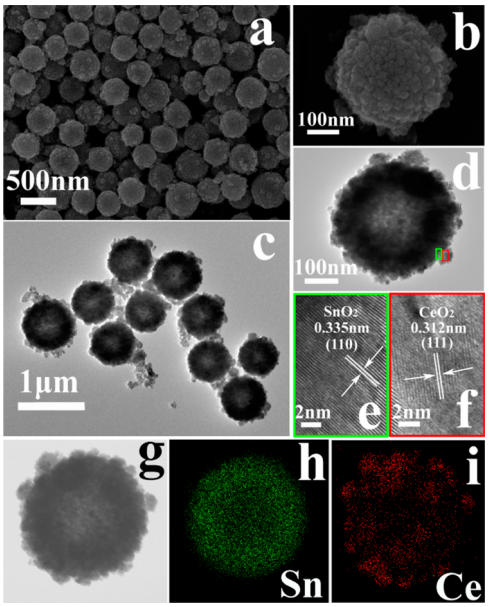

Figure 3. (a, b) Typical FESEM images of CeO_2/SnO_2 composites; (c, d) typical TEM image of CeO_2/SnO_2 composites; (e, f) high-resolution TEM images from marked fringe of panel d; (g) scanning TEM image and (h, i) the corresponding elemental mapping images of Sn and Ce.

The measured results of HRTEM were in accordance with the results of XRD.

3.2. Composition Analysis. The investigated results of XPS were carried out in Figure 4, which demonstrated the surface elemental composition and chemical status of the as-prepared CeO_2/SnO_2 composites. In the full range spectra (Figure S3a), peaks corresponding to Sn, Ce, O, and C were clearly observed, and no impurities could be found, which also indicated the high purity of CeO_2/SnO_2 composites. The Sn 3d spectrum (Figure 4a) had two strong peaks at the bending energies of 487.37 and 495.55 eV, which all belong to SnO_2 with a valence of +4.[35] The bending energies of Ce^{3+} and Ce^{4+} were displayed in Figure 4, panel b. In this figure, 883.69 eV, 888.93 eV, 900.15 eV, 907.90 eV, and 917.97 eV peaks were attributed to Ce^{4+}, while 885.70 eV, 898.96 eV, and 902.45 eV were the characteristic peaks of Ce^{3+} ions, which demonstrated that there was a certain amount of Ce^{3+} existence in CeO_2/SnO_2 composites.[36] In comparison to the Ce^{3+} in CeO_2 nanoparticles, the relative percentages of Ce^{3+} were displayed in Table S1, from which we could find that the content of Ce^{3+} in the composites (36.39%) was higher than pure CeO_2 nanoparticles (16.93%). This phenomenon may be due to the unique properties of ceria oxide. (I) Oxygen in CeO_2 is much more active, and lattice oxygen is highly mobile, which leads to the facile creation of defeats such as oxygen vacancies. (II) CeO_2 could act as an excellent promoter and has high oxygen transfer ability.[37,38] When CeO_2 is decorated on the surface of SnO_2, the unstable lattice oxygen may transfer to the surface of SnO_2 and be absorbed on it, which may lead to the creation of oxygen vacancies. Because Ce^{4+} is a scavenger of electrons and easily traps electrons, the electrons left by lattice oxygen combine with Ce^{4+} and form Ce^{3+}.[39,40] As for surface resistance-type metal oxide semiconductors, the ability of the sensing material to absorb and ionize oxygen species is fundamental to the performance of sensors. To verify the status of oxygen species of the as-prepared single-component

DOI: 10.1021/acsami.6b00169
ACS Appl. Mater. Interfaces XXXX, XXX, XXX−XXX

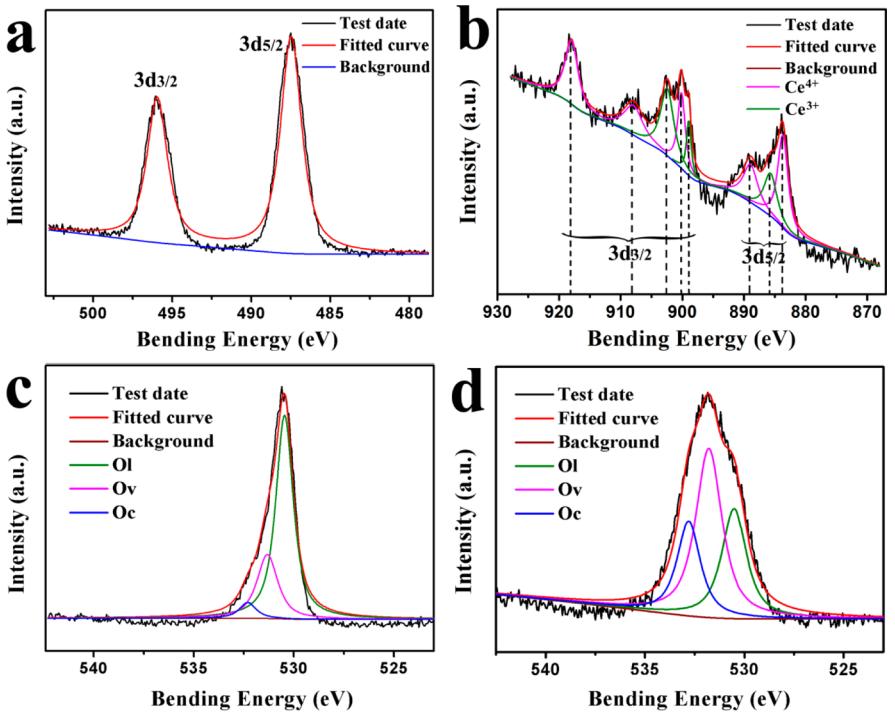

Figure 4. XPS analyses of (a) Sn 3d; (b) Ce 3d of CeO_2/SnO_2 composites; (c) O 1s spectra of single-component SnO_2 hollow spheres. (d) O 1s of the as-prepared CeO_2/SnO_2 composites.

SnO_2 hollow spheres and CeO_2/SnO_2 composites, the XPS spectrum of O 1s exhibited in Figure 4, panels c and d, respectively, in which curves all could be decomposed into three fitted peaks, indicates that there are significant differences between oxygen states on the surface of the samples. The O_L component was attributed to the lattice oxygen species, the middle of the three peaks was O_V component in oxygen-vacancy regions within the SnO_2 and CeO_2, and the O_C component was identified to chemisorbed and dissociated oxygen species.[41] Their center position and the relative percentage of each peak were listed in Table 1. It can be observed from Table 1 that the relative percentages of O_V and O_C in CeO_2/SnO_2 composites were increased compare with single-component SnO_2 hollow spheres. The enhancement of O_V was conformed to the increase content of Ce^{3+} in CeO_2/SnO_2 composites. We could estimate the oxygen-chemisorbed ability of different samples according to the intensity of O_C component in the O 1s XPS peak. For the different samples, the relative percentages of the O_C component were about 5.17% (CeO_2 nanoparticles in Table S2), 14.41% (SnO_2 hollow spheres) and 23.47% (CeO_2/SnO_2 composites), respectively. These results revealed that the CeO_2/SnO_2 composites had the highest ability for adsorbing the ionized oxygen species. Therefore, the extraordinary ability of chemisorbing oxygen greatly contributes to the high-performance gas sensing toward target gases.

Table 1. Fitting Results of O 1s XPS Spectra of the Three Samples

sample	oxygen species	binding energy (eV)	relative percentage (%)
SnO_2	O_L (Sn−O)	530.46	68.97%
hollow	O_V (vacancy)	531.32	25.86%
spheres	O_C (chemisorbed)	532.30	5.17%
CeO_2/SnO_2 composites	O_L (Sn−O and Ce−O)	530.52	29.18%
	O_V (vacancy)	531.79	47.34%
	O_C (chemisorbed)	532.80	23.47%

4. GAS SENSING APPLICATIONS

4.1. Fabrication and Sensing Measurement System of Gas Sensor. To demonstrate the potential applications of the as-synthesized materials, the gas sensors were fabricated as follows: the as-prepared products were coated onto an ceramic tube to develop a sensing film. After that, the devices were calcined at 400 °C for 2 h for the purpose of improving the stability of the gas sensor. A Ni−Cr alloy coil was inserted through the alumina tube to control the operating temperature of the sensor by controlling the heating current. Finally, the sensor was welded on a hexagon socket as shown in Figure S1. Gas-sensing properties of the as-prepared products were determined in a closed glass chamber (1 L in volume), and the sensor was put into the chambers, which were filled with targets gases by using a microinjector. The response is defined as R_a/R_g; R_a and R_g are the resistances of the sensors in air and in target gas, respectively.

4.2. Gas-Sensing Properties. As is well-known, the operating temperature of a semiconductor gas sensor has a high influence on the sensing properties. Therefore, a function of gas response to operating temperatures of sensors based on SnO_2 hollow spheres and CeO_2/SnO_2 composites to 100 ppm ethanol gas was carried out in Figure 5. At the beginning, the response of the sensor increased with the operating temperature, which may result from two factors. The one is that the species of adsorbed oxygen on the surface of the materials changed along with the temperature. The other is that the gas molecule could overcome the activation energy barrier of the surface reaction as the temperature increased.[42,43] Subsequently, the maximal of pure SnO_2 hollow spheres was 16 at

DOI: 10.1021/acsami.6b00169
ACS Appl. Mater. Interfaces XXXX, XXX, XXX−XXX

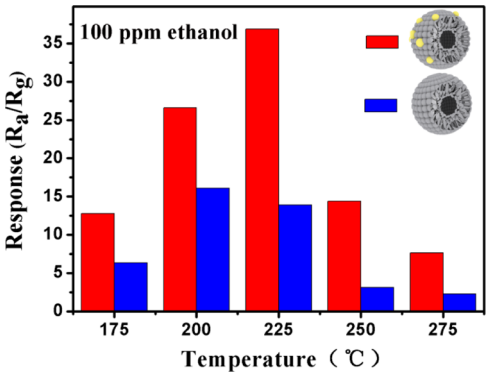

Figure 5. Response of pure hollow SnO_2 spheres and CeO_2/SnO_2 composites at various operating temperature to 100 ppm ethanol.

the temperature of 200 °C. In contrast with single-component SnO_2, the response of the sensor based on CeO_2/SnO_2 composites reached a maximum value of 37, which was 2.65-times higher than the sensor based on single-component SnO_2 hollow spheres of 13.7 at the same operating temperature of 225 °C to 100 ppm ethanol. However, the response of pure CeO_2 nanoparticles is much lower than the other two sensors (Figure S4). It just went to show the enhancement effect of CeO_2 to the response of SnO_2 hollow spheres. After the maximal value, the response decreased with further increasing the operating temperature. This decrease in the response might be caused by the number of ethanol adsorption active sites decreasing. Another possibility was that the adsorption ability of target gas molecules was lower than that of desorption and led to the utilization rate of sensing material decreasing at such high temperatures. Thus, the resistance change would be decreased at higher temperature.[44−46]

The response and recovery properties are additional major parameters for gas sensors. It is necessary for sensors to have a excellent response and recovery characterization in practical application. Response and recovery times are defined as the time taken by the sensor to achieve 90% of the total resistance change in the case of adsorption and desorption, respectively. Figure 6, panel a shows the dynamic response and recovery curves of the CeO_2/SnO_2 composites to 100 ppm ethanol at 225 °C. It can be found that when the sensor was exposed to ethanol, the resistance descended immediately. The time taken was only 2 s in this process. The large surface area (Figure S5) of the hollow spheres provided sufficient active sites, which result in the fast response. Then the ethanol gas diffused through the sensing layer and occupied the remaining surface reaction sites, which leads to the resistance reached a steady. However, the resistance gradually increased (70 s) to a near baseline level as the sensor was exposed to air atmosphere, which might result from the time taken by the process of the desorption of oxidation ethanol molecules and oxygen absorbed on the surface of the materials again. Figure 6, panel b presents six reversible response cycles that confirmed the CeO_2/SnO_2 composites had a stable and repeatable characteristic as sensing material. Table 2 shows the sensing performances comparison between CeO_2/SnO_2 composites hollow spheres and some ethanol gas sensors based on SnO_2. The results confirmed that CeO_2/SnO_2 composites hollow spheres had a higher response and a lower temperature, which mean they may be more suitable for gas sensor.

The dynamic response of CeO_2/SnO_2 composites and the pure SnO_2 hollow spheres under different concentration from 10−100 ppm of ethanol at 225 °C were revealed in Figure 7. With the increased concentration of ethanol, the response of pure SnO_2 hollow spheres and CeO_2/SnO_2 composites also increased, and it could be observed clearly that the response enhanced significantly after the CeO_2 composited with the SnO_2 hollow spheres. It could be observed that the response of the two sensors showed an approximately linear increase under ethanol concentration ranging from 10−100 ppm. In the meantime, these two kinds of gas sensors exhibited excellent response and recovery characteristics to different concentrations of ethanol.

In terms of semiconductor gas sensors, selectivity is another important criterion. Figure 8 reveals the sensitivity of the sensors using the SnO_2 hollow spheres and CeO_2/SnO_2 composites to some common interfering gases including 100 ppm ethanol, acetone, methanol, formaldehyde, toluene, and 10 ppm of H_2S. The sensitivites to those target gases were all tested at the same temperature of 225 °C. Obviously, the sensor based on CeO_2/SnO_2 composites showed enhanced responses to target gases, and the response to ethanol was 37, higher than those for other testing gases. The response was 25.7, 23.4, 3.9, and 5.4 for 100 ppm of acetone, methanol, formaldehyde, toluene, and benzene, respectively. For 10 ppm of H_2S gas, it was 2.0. In other words, CeO_2/SnO_2 composites materials have selectivity toward ethanol over the other gases at 225 °C.

4.3. Gas-Sensing Mechanism. The enhanced gas-sensing properties of composites are likely to result from the following reasons. A schematic diagram of the composites in the air and ethanol gases is shown in Figure 9.

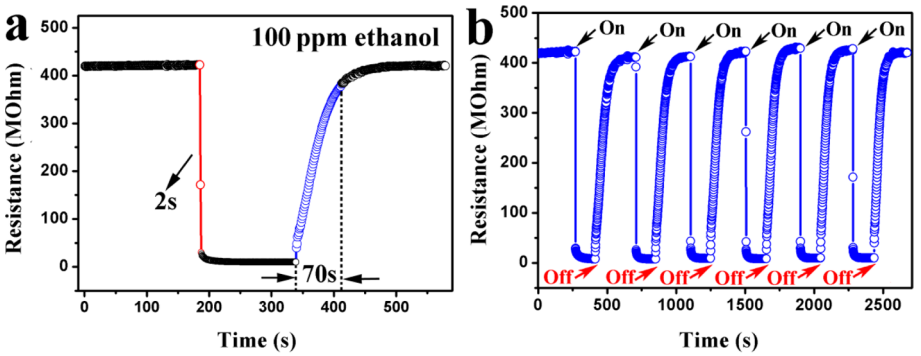

Figure 6. (a) Response and recovery curves of CeO_2/SnO_2 composites and (b) six reversible cycles to 100 ppm ethanol at 225 °C.

DOI: 10.1021/acsami.6b00169
ACS Appl. Mater. Interfaces XXXX, XXX, XXX−XXX

Table 2. Comparison of Gas-Sensing Performances of Ethanol Gas Sensors Based on SnO_2

sensing material	technologies	operating temperature (°C)	ethanol concentration (ppm)	response	response time	references
mesoporous ZnO−SnO_2 nanofibers	electrospinning	300 °C	100	21.88	3 s	47
Fe_2O_3/SnO_2 semiconductor composites	hydrothermal	250 °C	100	18		26
Ce-doped SnO_2 thin films	sol−gel method	300 °C	800	9		48
NiO-SnO_2 hollow spheres	hydrothermal	450 °C	50	2.58	2 s	49
CeO_2/SnO_2 composites hollow spheres	hydrothermal	225 °C	100	37	2 s	this work

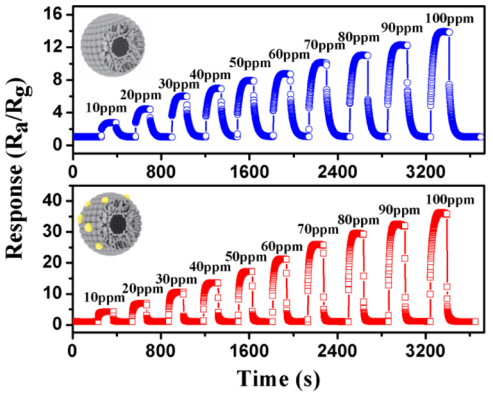

Figure 7. Responses of the sensors based on SnO_2 hollow spheres and CeO_2/SnO_2 composites as a function of ethanol concentrations ranging from 10−100 ppm at 225 °C.

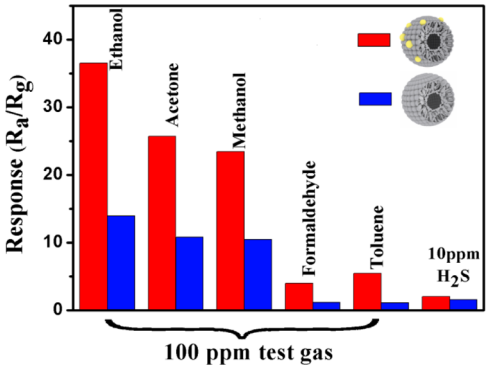

Figure 8. Comparison of the responses to various test gases at 225 °C.

First, it is well-known that the gas-sensing ability of semiconductor oxides is closely associated with their capacity of adsorbing oxygen on the surface of the materials. When the gas sensor is exposed to air, oxygen molecules will be adsorbed onto the surfaces of the sensing materials by transferring electrons to the surface of the semiconductor to decrease the electron concentration sequentially, and the resistance of the sensor increased. The commonly chemisorbed oxygen ions is O_2^- at low temperatures, but O^- and O^{2-} are commonly chemisorbed at higher temperatures.[42,43] When the material is contacted with reduction gas, ethanol as an example, adsorbed oxygen could react with ethanol gas molecules on the surface of the material, and electrons trapped in the adsorbed oxygen species would be released back into the conduction band of the semiconductor oxides and result in the increase of conductivity. In our study, both SnO_2 and CeO_2 are n-type semiconductor oxides; the heterojunction between them takes the principal place in the response enhancement of composites. A possible energy band structure diagram of the CeO_2/SnO_2 heterojunction is presented in Figure 9, and the work function of CeO_2 (4.69 eV) is smaller than SnO_2 (4.90 eV);[50−52] electrons will flow from CeO_2 to SnO_2, which will result in the formation of the hole depletion layer in CeO_2 nanoparticles and electron accumulation layer on the surface of SnO_2. This will result in the rised amount of chemisorbed oxygen, which conforms to the XPS results. Because the adsorbing oxygen traps a lot of electrons, a high barrier between the two semiconductor oxides is generated and makes the composites have a higher resistance. Φ_{eff} is the effective barrier height. On the basis of the above experimental results and the theory analysis, the increasing number of electrons on the surface of oxide materials will lead to the increase of adsorbed oxygen. Ethanol would extract more oxygen from the gas sensing materials containing CeO_2 than the SnO_2 without CeO_2. As the sensors are exposed to ethanol gas, more electrons are released back to SnO_2 conduction band, and the barrier height will be decreased a great deal due to the higher concentration of electrons; thereby, a low resistance is obtained. This means that the sensitivity of composites to ethanol can be enhanced.

Second, the results of XPS have found the existence of Ce^{3+}, and the amount of oxygen vacancy increased after CeO_2 nanoparticles decorated on the surface of SnO_2 hollow spheres. Many people support that the oxygen-defect formation is accompanied by localization of the electrons left behind in Ce 4f states, leading to the formation of two Ce^{3+} ions while still maintaining a cubic fluorite crystal structure.[53,54] According to eq 1,

$$2Ce^{4+} + O^{2-} = 2Ce^{3+} + Vo^{\bullet\bullet} + 1/2O_2 \quad (1)$$

Vo is the abbreviation of the O vacancy with two units of negative charges, and it could be electron donor due to the ability of releasing those negative charges to the conduction band, which will result in the rise of electron concentration. Thus, the existence of a larger amount of vacancies in CeO_2/SnO_2 composites induces stronger adsorptions of oxygen, leading to an increase of the sensitivity.

Third, in accordance with reducing gases, could transfer Ce^{4+} to Ce^{3+} on the surface of CeO_2,[37,55,56] and the process of ethanol reacting with CeO_2 is shown in Figure 9, and the chemical equation might be like eq 2:

$$12CeO_2 + C_2H_5OH = 2CO_2 + 3H_2O + 6Ce_2O_3 \quad (2)$$

For the reason for the generation of Ce^{3+} and Vo, the surface oxygen vacancies can be electron donor, and there would be more electrons flow from CeO_2 surface to SnO_2 surface leading directly to the increase of conductivity. As for the pure CeO_2 nanoparticles, electron would be trapped by Ce^{4+}, which means a high resistance and low response would occur. When the sensor is put back into air, the electrons combine with oxygen on the surface again, and the following reaction 3 will occur:

$$[2Ce^{3+}, Vo^{\bullet\bullet}] + O_2 \rightarrow [Ce^{4+}, Ce^{3+}, O^{2-}] \quad (3)$$

DOI: 10.1021/acsami.6b00169
ACS Appl. Mater. Interfaces XXXX, XXX, XXX−XXX

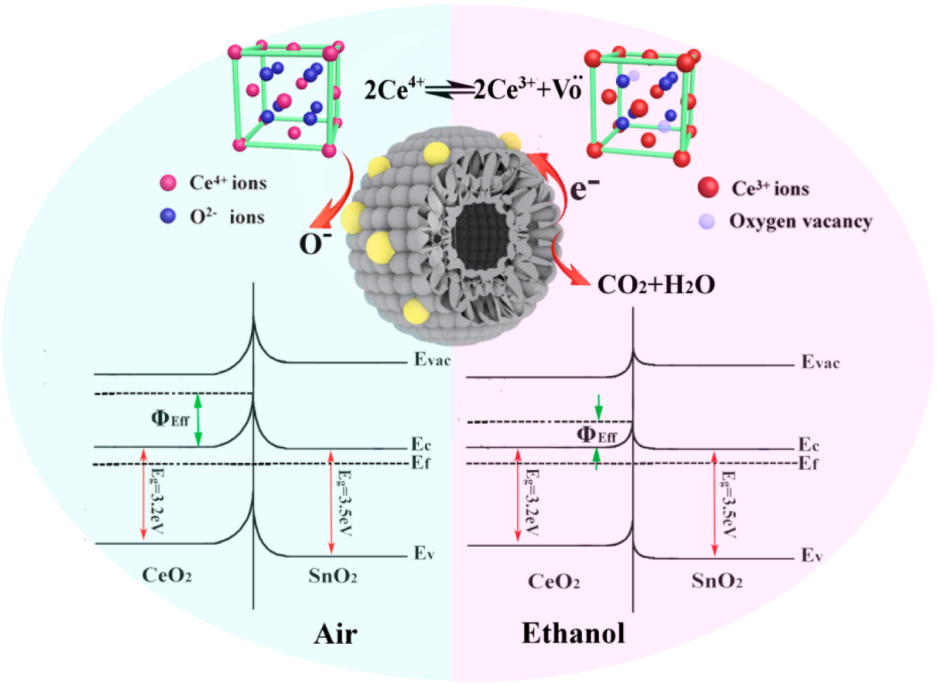

Figure 9. Schematic diagram illustrating the plausible reason for gas sensing properties and the energy band structure of CeO_2/SnO_2 heterostructure in air and ethanol gases.

This means the decrease of Ce^{3+} and Vo will occur. They are all led to the reduction of electron concentration and the resistance rise back. According to what has been discussed above, this explanation may be the origin of the improvement in gas sensing performance.

5. CONCLUSIONS

In summary, the synthesized method of CeO_2 nanoparticles decorated on SnO_2 hollow spheres had been successfully prepared by a two-step hydrothermal route. The morphology and structure characteristics were demonstrated by FESEM and TEM observations. XPS results of the composites demonstrated the existence of Ce^{3+} and the enhanced amount of both chemisorbed oxygen and oxygen vacancy compared with the pure SnO_2, which provides direct evidence to the enhancement of gas sensing properties. The applications in gas sensor of as-prepared materials were studied. The CeO_2/SnO_2 composites exhibited excellent enhanced sensitivity toward ethanol, which was about 2.65-times higher than pure SnO_2 hollow spheres. The enhancement of gas sensing properties was attributed to the formation of heterojunction between SnO_2 and CeO_2 and the conversion between Ce^{3+} and Ce^{4+}. Our results suggested that the CeO_2/SnO_2 composites hollow spheres are promising candidates for high performance gas sensors.

■ ASSOCIATED CONTENT

Supporting Information

The Supporting Information is available free of charge on the ACS Publications website at DOI: 10.1021/acsami.6b00169.

Gas sensor schematic diagram; EDS elemental maps of SnO_2/CeO_2 composites; XPS analyses of full range spectra, Ce 3d, and O 1s spectra of single-component CeO_2 nanoparticles; fitting results of Ce 3d XPS spectra of CeO_2/SnO_2 composites and pure CeO_2 nanoparticles; fitting results of O 1s XPS spectra of the CeO_2 nanoparticles; response of CeO_2 nanoparticles at various operating temperature to 100 ppm ethanol; typical N_2 adsorption/desorption isotherms and pore size distribution curves of SnO_2 hollow spheres and CeO_2/SnO_2 composites (PDF)

■ AUTHOR INFORMATION

Corresponding Authors

*E-mail: spmaster2008@163.com. Phone: +86-431-85167808. Fax: +86-431-85167808.
*E-mail: lugy@jlu.edu.cn.

Notes

The authors declare no competing financial interest.

■ ACKNOWLEDGMENTS

This research work is financially supported by the National Nature Science Foundation of China (Nos. 61374218, 61134010, 61327804, 61304242, and 61474057), Program for Chang Jiang Scholars and Innovative Research Team in University (No. IRT13018), and National High-Tech Research and Development Program of China (863 Program, Nos. 2013AA030902 and 2014AA06A505).

■ ABBREVIATIONS

HMT, hexamethylenetetramine
XRD, X-ray powder diffraction
FESEM, field-emission scanning electron microscopy
TEM, transmission electron microscopy
HRTEM, high-resolution transmission electron microscopy
EDS, energy dispersive spectroscopy
XPS, X-ray photoelectron spectroscopy

■ REFERENCES

(1) Li, L.; He, S. J.; Liu, M.; Zhang, C. M.; Chen, W. Three-Dimensional Mesoporous Graphene Aerogel-Supported SnO_2 Nano-

DOI: 10.1021/acsami.6b00169
ACS Appl. Mater. Interfaces XXXX, XXX, XXX−XXX

crystals for High-Performance NO_2 Gas Sensing at Low Temperature. *Anal. Chem.* **2015**, *87*, 1638−1645.
(2) Wetchakun, K.; Samerjai, T.; Tamaekong, N.; Liewhiran, C.; Siriwong, C.; Kruefu, V.; Wisitsoraat, A.; Tuantranont, A.; Phanichphant, S. Semiconducting Metal Oxides as Sensors for Environmentally Hazardous Gases. *Sens. Actuators, B* **2011**, *160*, 580−591.
(3) Li, X. W.; Zhou, X.; Guo, H.; Wang, C.; Liu, J. Y.; Sun, P.; Liu, F.; Lu, G. Design of Au@ZnO Yolk−Shell Nanospheres with Enhanced Gas Sensing Properties. *ACS Appl. Mater. Interfaces* **2014**, *6*, 18661−18667.
(4) Zhao, J.; Yang, T. L.; Liu, Y. P.; Wang, Z. Y.; Li, X. W.; Sun, Y. F.; Du, Y.; Li, Y. C.; Lu, G. Y. Enhancement of NO_2 Gas Sensing Response Based on Ordered Mesoporous Fe-doped In_2O_3. *Sens. Actuators, B* **2014**, *191*, 806−812.
(5) Li, L.; Zhang, C. M.; Chen, W. Fabrication of SnO_2−SnO Nanocomposites with P−N Heterojunctions for the Low-Temperature Sensing of NO_2 Gas. *Nanoscale* **2015**, *7*, 12133−12142.
(6) Ponzoni, A.; Russo, V.; Bailini, A.; Casari, C. S.; Ferroni, M.; Li Bassi, A.; Migliori, A.; Morandi, V.; Ortolani, L.; Sberveglieri, G.; Bottani, C. E. Structural and Gas-Sensing Characterization of Tungsten Oxide Nanorods and Nanoparticles. *Sens. Actuators, B* **2011**, *153*, 340−346.
(7) Wang, D.; Chu, X. F.; Gong, M. L. Gas-sensing Properties of Sensors Based on Single-crystalline SnO_2 Nanorods Prepared by a Simple Molten-salt Method. *Sens. Actuators, B* **2006**, *117*, 183−187.
(8) Ramgir, N. S.; Sharma, P. K.; Datta, N.; Kaur, M.; Debnath, A. K.; Aswal, D. K.; Gupta, S. K. Room Temperature H_2S Sensor Based on Au Modified ZnO Nanowires. *Sens. Actuators, B* **2013**, *186*, 718−726.
(9) You, L.; He, X.; Wang, D.; Sun, P.; Sun, Y. F.; Liang, X. S.; Du, Y.; Lu, G. Y. Ultrasensitive and Low Operating Temperature NO_2 Gas Sensor Using Nanosheets Assembled Hierarchical WO_3 Hollow Microspheres. *Sens. Actuators, B* **2012**, *173*, 426−432.
(10) Manjula, P.; Boppella, R.; Manorama, S. V. A Facile and Green Approach for the Controlled Synthesis of Porous SnO_2 Nanospheres: Application as an Efficient Photocatalyst and an Excellent Gas Sensing Material. *ACS Appl. Mater. Interfaces* **2012**, *4*, 6252−6260.
(11) Zhang, H.; Wu, R.; Chen, Z.; Liu, G.; Zhang, Z.; Jiao, Z. Self-Assembly Fabrication of 3D Flower-Like ZnO Hierarchical Nanostructures and Their Gas Sensing Properties. *CrystEngComm* **2012**, *14*, 1775−1782.
(12) Sun, P.; Zhao, W.; Cao, Y.; Guan, Y.; Sun, Y.; Lu, G. Porous SnO_2 Hierarchical Nanosheets: Hydrothermal Preparation, Growth Mechanism, and Gas Sensing Properties. *CrystEngComm* **2011**, *13*, 3718.
(13) Song, H. J.; Jia, X. H.; Qi, H.; Yang, X. F.; Tang, H.; Min, C. Y. Flexible Morphology-Controlled Synthesis of Monodisperse a-Fe_2O_3 Hierarchical Hollow Microspheres and Their Gas-Sensing Properties. *J. Mater. Chem.* **2012**, *22*, 3508−3516.
(14) Kim, K. M.; Choi, K.; Jeong, H. M.; Kim, H. J.; Kim, H. R.; Lee, J. H. Highly Sensitive and Selective Trimethylamine Sensors Using Ru-doped SnO_2 Hollow Spheres. *Sens. Actuators, B* **2012**, *166-167*, 733−738.
(15) Zhang, H. G.; Zhu, Q. S.; Zhang, Y.; Wang, Y.; Zhao, L.; Yu, B. One-Pot Synthesis and Hierarchical Assembly of Hollow Cu_2O Microspheres with Nanocrystals-Composed Porous Multishell and Their Gas-Sensing Properties. *Adv. Funct. Mater.* **2007**, *17*, 2766−2771.
(16) Ge, L.; Jing, X. Y.; Wang, J.; Wang, J.; Jamil, S.; Liu, Q.; Liu, F. C.; Zhang, M. L. Trisodium Citrate Assisted Synthesis of ZnO Hollow Spheres Via a Facile Precipitation Route and Their Application as Gas Sensor. *J. Mater. Chem.* **2011**, *21*, 10750−10754.
(17) Lou, X. W.; Archer, L. A.; Yang, Z. C. Hollow Micro/Nanostructures: Synthesis and Applications. *Adv. Mater.* **2008**, *20*, 3987−4019.
(18) Wang, Y. L.; Jiang, X. C.; Xia, Y. N. A Solution Phase Precursor Route to Polycrystalline SnO_2 Nanowires That Can be Used for Gas Sensing under Ambient Conditions. *J. Am. Chem. Soc.* **2003**, *125*, 16176−16177.
(19) Hyodo, T.; Abe, S.; Shimizu, Y.; Egashira, M. Gas-sensing Properties of Ordered Mesoporous SnO_2 and Effects of Coatings Thereof. *Sens. Actuators, B* **2003**, *93*, 590−600.
(20) Sun, P.; Zhou, X.; Wang, C.; Wang, B.; Xu, X. M.; Lu, G. Y. One-step Synthesis and Gas Sensing Properties of Hierarchical Cd-doped SnO_2 Nanostructures. *Sens. Actuators, B* **2014**, *190*, 32−39.
(21) Guan, Y.; Wang, D. W.; Zhou, X.; Sun, P.; Wang, H.; Ma, J.; Lu, G. Y. Hydrothermal Preparation and Gas Sensing Properties of Zn-doped SnO_2 Hierarchical Architectures. *Sens. Actuators, B* **2014**, *191*, 45−52.
(22) Firooz, A. A.; Hyodo, T.; Mahjoub, A. R.; Khodadadi, A. A.; Shimizu, Y. Synthesis and Gas-sensing Properties of Nano and Mesoporous MoO_3-doped SnO_2. *Sens. Actuators, B* **2010**, *147*, 554−560.
(23) Xue, X. Y.; Xing, L. L.; Chen, Y. J.; Shi, S. L.; Wang, Y. G.; Wang, T. H. Synthesis and H_2S Sensing Properties of CuO−SnO_2 Core/Shell PN-Junction Nanorods. *J. Phys. Chem. C* **2008**, *112*, 12157−12160.
(24) Chu, D. W.; Zeng, Y. P.; Jiang, D. L.; Masuda, Y. In_2O_3-SnO_2 Nano-Toasts and Nanorods: Precipitation Preparation, Formation Mechanism, and Gas Sensitive Properties. *Sens. Actuators, B* **2009**, *137*, 630−636.
(25) Wang, C.; Cheng, X. Y.; Zhou, X.; Sun, P.; Hu, X. L.; Shimanoe, K.; Lu, G. Y.; Yamazoe, N. Hierarchical α-Fe_2O_3/NiO Composites with a Hollow Structure for a Gas Sensor. *ACS Appl. Mater. Interfaces* **2014**, *6*, 12031−12037.
(26) Sun, P.; Zhou, X.; Wang, C.; Shimanoe, K.; Lu, G. Y.; Yamazoe, N. Hollow SnO_2/a-Fe_2O_3 Spheres with a Double-shell Structure for Gas Sensors. *J. Mater. Chem. A* **2014**, *2*, 1302−1308.
(27) Nguyen, T. B.; Deloume, J. P.; Perrichon, V. Study of the Redox Behaviour of High Surface Area CeO_2−SnO_2 Solid Solutions. *Appl. Catal., A* **2003**, *249*, 273−284.
(28) Ma, Y.; Wang, X. D.; Li, S. H.; Toprak, M. S.; Zhu, B.; Muhammed, M. Samarium-Doped Ceria Nanowires: Novel Synthesis and Application in Low-Temperature Solid Oxide Fuel. *Adv. Mater.* **2010**, *22*, 1640−1644.
(29) Izu, N.; Oh-hori, N.; Shin, W.; Matsubara, I.; Murayama, N.; Itou, M. Response Properties of Resistive Oxygen Sensors Using $Ce_{1-x}ZrxO_2$ (x = 0.05, 0.10) Thick Films in Propane Combustion Gas. *Sens. Actuators, B* **2008**, *130*, 105−109.
(30) Chen, Y.; Long, R. W. Polishing Behavior of PS/CeO_2 Hybrid Microspheres with Controlled Shell Thickness on Silicon Dioxide CMP. *Appl. Surf. Sci.* **2011**, *257*, 8679−8685.
(31) Mai, H. X.; Sun, L. D.; Zhang, Y. W.; Si, R.; Feng, W.; Zhang, H. P.; Liu, H. C.; Yan, C. H. Shape-Selective Synthesis and Oxygen Storage Behavior of Ceria Nanopolyhedra, Nanorods, and Nanocubes. *J. Phys. Chem. B* **2005**, *109*, 24380−24385.
(32) Zhang, J.; Kumagai, H.; Yamamura, K.; Ohara, S.; Takami, S.; Morikawa, A.; Shinjoh, H.; Kaneko, K.; Adschiri, T.; Suda, A. Extra-Low-Temperature Oxygen Storage Capacity of CeO_2 Nanocrystals with Cubic Facets. *Nano Lett.* **2011**, *11*, 361−364.
(33) Jiang, Z. W.; Guo, Z.; Sun, B.; Jia, Y.; Li, M. Q.; Liu, J. H. Highly Sensitive and Selective Butanone Sensors Based on Cerium-doped SnO_2 Thin Films. *Sens. Actuators, B* **2010**, *145*, 667−673.
(34) Qin, W. F.; Xu, L.; Song, J.; Xing, R. Q.; Song, H. W. Highly Enhanced Gas Sensing Properties of Porous SnO_2−CeO_2 Composite Nanofibers Prepared by Electrospinning. *Sens. Actuators, B* **2013**, *185*, 231−237.
(35) Yang, D. J.; Kamienchick, I.; Youn, D. Y.; Rothschild, A.; Kim, I. Ultrasensitive and Highly Selective Gas Sensors Based on Electrospun SnO_2 Nanofibers Modified by Pd Loading. *Adv. Funct. Mater.* **2010**, *20*, 4258−4264.
(36) Korsvik, C.; Patil, S.; Seal, S.; Self, W. T. Superoxide Dismutase Mimetic Properties Exhibited by Vacancy Engineered Ceria Nanoparticles. *Chem. Commun.* **2007**, 1056−1058.
(37) Agarwal, S.; Zhu, X.; Hensen, E. J. M.; Mojet, B. L.; Lefferts, L. Surface-Dependence of Defect Chemistry of Nanostructured Ceria. *J. Phys. Chem. C* **2015**, *119*, 12423−12433.

DOI: 10.1021/acsami.6b00169
ACS Appl. Mater. Interfaces XXXX, XXX, XXX−XXX

(38) Esch, F.; Fabris, S.; Zhou, L.; Montini, T.; Africh, C.; Fornasiero, P.; Comelli, G.; Rosei, R. Electron Localization Determines Defect Formation on Ceria Substrates. *Science* **2005**, *309*, 752−755.
(39) Chen, J. J.; Zhou, N.; Wang, H. Y.; Peng, Z. G.; Li, H. Y.; Tang, Y. G.; Liu, K. Synergistically Enhanced Oxygen Reduction Activity of MnOx−CeO_2/Ketjenblack Composites. *Chem. Commun.* **2015**, *51*, 10123.
(40) Ma, T. Y.; Yuan, Z. Y.; Cao, J. J. Hydrangea-like Meso/macroporous ZnO−CeO_2 Binary Oxide Materials: Synthesis, Photocatalysis and CO Oxidation. *Eur. J. Inorg. Chem.* **2010**, *2010*, 716−724.
(41) Dupin, J. C.; Gonbeau, D.; Vinatier, P.; Levasseur, A. Systematic XPS Studies of Metal Oxides, Hydroxides, and Peroxides. *Phys. Chem. Chem. Phys.* **2000**, *2*, 1319−1324.
(42) Belmonte, J. C.; Manzano, J.; Arbiol, J.; Cirera, A.; Puigcorbe, J.; Vila, A.; Sabate, N.; Gracia, I.; Cane, C.; Morante, J. R. Micromachined Twin Gas Sensor for CO and O_2 Quantification Based on Catalytically Modified Mano-SnO_2. *Sens. Actuators, B* **2006**, *114*, 881−892.
(43) Yamazoe, N.; Sakai, G.; Shimanoe, K. Oxide Semiconductor Gas Sensors. *Catal. Surv. Asia* **2003**, *7*, 63−75.
(44) Ju, D. X.; Xu, H. Y.; Qiu, Z. W.; Guo, J.; Zhang, J.; Cao, B. Q. Highly Sensitive and Selective Triethylamine-sensing Properties of Nanosheets Directly Grown on Ceramic Tube by Forming NiO/ZnO PN Heterojunction. *Sens. Actuators, B* **2014**, *200*, 288−296.
(45) Ju, D. X.; Xu, H. Y.; Zhang, J.; Guo, J.; Cao, B. Q. Direct Hydrothermal Growth of ZnO Nanosheets on Electrode for Ethanol Sensing. *Sens. Actuators, B* **2014**, *201*, 444−451.
(46) Bie, L.; Yan, X. N.; Yin, J.; Duan, Y. Q.; Yuan, Z. H. Nanopillar ZnO Gas Sensor for Hydrogen and Ethanol. *Sens. Actuators, B* **2007**, *126*, 604−608.
(47) Song, X.; Wang, Z.; Liu, Y.; Wang, C.; Li, L. A Highly Sensitive Ethanol Sensor Based on Mesoporous ZnO−SnO_2 Nanofibers. *Nanotechnology* **2009**, *20*, 075501.
(48) Pourfayaz, F.; Khodadadi, A.; Mortazavi, Y.; Mohajerzadeh, S. S. CeO_2 Doped SnO_2 Sensor Selective to Ethanol in Presence of CO, LPG and CH_4. *Sens. Actuators, B* **2005**, *108*, 172−176.
(49) Cantalini, C.; Post, M.; Buso, D.; Guglielmi, M.; Martucci, A. Gas Sensing Properties of Nanocrystalline NiO and Co_3O_4 in Porous Silica Sol−gel Films. *Sens. Actuators, B* **2005**, *108*, 184−192.
(50) Chen, Y. J.; Xiao, G.; Wang, T. S.; Zhang, F.; Ma, Y.; Gao, P.; Zhu, C.-L.; Zhang, E.; Xu, Z.; Li, Q.-H. Synthesis and Enhanced Gas Sensing Properties of Crystalline CeO_2/TiO_2 Core/shell Nanorods. *Sens. Actuators, B* **2011**, *156*, 867−874.
(51) Fangxin, L.; Chengyun, W.; Qingde, S.; Tianpeng, Z.; Guiwen, Z. Optical Properties of Nanocrystalline Ceria. *Appl. Opt.* **1997**, *36*, 2796−2798.
(52) Zhang, Y. C.; Du, Z. N.; Li, K. W.; Zhang, M.; Dionysiou, D. D. High-Performance Visible-Light-Driven SnS_2/SnO_2 Nanocomposite Photocatalyst Prepared via Insitu Hydrothermal Oxidation of SnS_2 Nanoparticles. *ACS Appl. Mater. Interfaces* **2011**, *3*, 1528−1537.
(53) Deshpande, S.; Patil, S.; Kuchibhatla, S.; Seal, S. Size Dependence Variation in Lattice Parameter and Valence States in Nanocrystalline Cerium Oxide. *Appl. Phys. Lett.* **2005**, *87*, 133113.
(54) Tanner, P. A.; Mak, S. K.; Edelstein, N. M.; Murdoch, K. M.; Liu, G.; Huang, J.; Seijo, L.; Barandiaran, Z. Absorption and Emission Spectra of Ce^{3+} in Elpasolite Lattices. *J. Am. Chem. Soc.* **2003**, *125*, 13225−13233.
(55) Ganduglia-Pirovano, M. V.; Hofmann, A.; Sauer, J. Oxygen Vacancies in Transition Metal and Rare Earth Oxides: Current State of Understanding and Remaining Challenges. *Surf. Sci. Rep.* **2007**, *62*, 219−270.
(56) Joy, N. A.; Nandasiri, M. I.; Rogers, P. H.; Jiang, W.; Varga, T.; Kuchibhatla, S. V. N. T.; Thevuthasan, S.; Carpenter, M. A. Selective Plasmonic Gas Sensing: H_2, NO_2, and CO Spectral Discrimination by a Single Au−CeO_2 Nanocomposite Film. *Anal. Chem.* **2012**, *84*, 5025−5034.

DOI: 10.1021/acsami.6b00169
ACS Appl. Mater. Interfaces XXXX, XXX, XXX−XXX